PAPER *Special Section on VLSI Design and CAD Algorithms*

Closed-Form Expressions for Crosstalk Noise and Worst-Case Delay on Capacitively Coupled Distributed RC Lines

Hiroshi KAWAGUCHI[†*a)], ***Nonmember***, **Danardono Dwi ANTONO**[†**], ***and*** **Takayasu SAKURAI**[†], ***Members***

SUMMARY Closed-form expressions for a crosstalk noise amplitude and worst-case delay in capacitively coupled two-line and three-line systems are derived assuming bus lines and other signal lines in a VLSI. Two modes are studied; a case that adjacent lines are driven from the same direction, and the other case that adjacent lines are driven from the opposite direction. Beside, a junction capacitance of a driver MOSFET is considered. The closed-form expressions are useful for circuit designers in an early stage of a VLSI design to give insight to interconnection problems. The expressions are extensively compared and fitted to SPICE simulations. The relative and absolute errors in the crosstalk noise amplitude are within 63.8% and 0.098 E (where E is a supply voltage), respectively. The relative error in the worst-case delay is less than 8.1%.

key words: *interconnection, crosstalk, coupled transmission lines, integrated circuit noise, delays*

1. Introduction

Interconnection related issues become more and more important in estimating VLSI behavior [1]. For instance, a coupling capacitance is getting comparable to a grounding capacitance, and crosstalk noise may cause malfunction and timing problem, particularly, in dynamic circuits. Even in static circuits, noise may generate unexpected glitches, which gives rise to timing and power issues as well.

Several attempts have been made to treat crosstalk noise and delay in capacitively coupled interconnections [2]–[7]. Although [2], [3] handle crosstalk noise in coupled RC lines, the interconnections are not distributed lines. [4] is limited to delay estimation in a two-line system. [5]–[7] describe both delay and crosstalk noise but do not give closed-form expression, which are useful for EDA implementation while it is too complicated for circuit designers. Moreover, they are restricted to the case that adjacent lines are driven from the same direction (hereafter, same-direction drive), and do not reflect on a junction capacitance of a driver MOSFET.

This paper extends analysis of crosstalk noise and worst-case delay to another general case that adjacent lines are driven from the opposition direction (hereafter, opposite-direction drive). In addition to the two-line system, we analyze a three-line system. The derived expressions are useful for circuit designers in estimating crosstalk noise and worst-case delay, and give insight to coupling related issues in an early stage of a VLSI design. Note that we do not consider an inductance, L, and mutual inductance, M, in this paper since they do not affect delay and crosstalk noise very much in future copper processes [8], [9].

This paper is organized as follows. In the next section, we will mention basic equations of capacitively coupled distribution lines. In Sects. 3 and 4, we will discuss crosstalk noise and worst-case delay in the same-direction and opposite-direction drive cases, respectively. Finally, a summary follows in Sect. 5.

2. Basic Equations

Figure 1 illustrates capacitively coupled distributed RC lines in a two-line system. It is governed by the following basic equation set;

$$\begin{cases} \dfrac{\partial^2 v_1(x,t)}{\partial x^2} = r_1(c_1+c_c)\dfrac{\partial v_1(x,t)}{\partial t} - r_1 c_c \dfrac{\partial v_2(x,t)}{\partial t} \\ \dfrac{\partial^2 v_2(x,t)}{\partial x^2} = r_2(c_2+c_c)\dfrac{\partial v_2(x,t)}{\partial t} - r_2 c_c \dfrac{\partial v_1(x,t)}{\partial t} \end{cases}, \quad (1)$$

where $v_i(x,t)$ $(i=1,2)$ is a voltage of the line i. r_i, c_i, and c_c are a resistance, a capacitance, and a coupling capacitance between the lines per unit length. Since a bus and other wiring structures laid out on a same level have a same resistance and capacitance per unit length, we hereafter assume $r_1 = r_2 = r$ and $c_1 = c_2 = c$. In this paper, we do not consider lines on different levels because lines on upper and lower levels cross at right angle, and a coupling capacitance between them is negligible.

In the three-line system in Fig. 2, the following equation set holds;

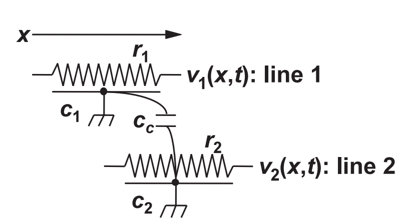

Fig. 1 Two distributed RC lines capacitively coupled (two-line system). The x-coordinate indicates position along lines. t is time.

Manuscript received March 12, 2007.
Manuscript revised June 14, 2007.
Final manuscript received August 8, 2007.

[†]The authors are with the Institute of Industrial Science, the University of Tokyo, Tokyo, 153-8505 Japan.
[*]Presently, with the Department of Computer and Systems Engineering, Kobe University.
[**]Presently, with Sony Corporation.
a) E-mail: kawapy@godzilla.kobe-u.ac.jp

DOI: 10.1093/ietfec/e90–a.12.2669

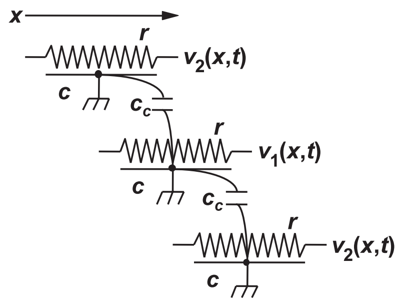

Fig. 2 Three distributed RC lines capacitively coupled (three-line system).

$$\begin{cases} \dfrac{\partial^2 v_1(x,t)}{\partial x^2} = r(c+2c_c)\dfrac{\partial v_1(x,t)}{\partial t} - 2rc_c\dfrac{\partial v_2(x,t)}{\partial t} \\ \dfrac{\partial^2 v_2(x,t)}{\partial x^2} = r(c+c_c)\dfrac{\partial v_2(x,t)}{\partial t} - rc_c\dfrac{\partial v_1(x,t)}{\partial t} \end{cases}. \quad (2)$$

(1) and (2) can be represented as follows;

$$\begin{cases} \dfrac{\partial^2 v_1(x,t)}{\partial x^2} = r(c+nc_c)\dfrac{\partial v_1(x,t)}{\partial t} - nrc_c\dfrac{\partial v_2(x,t)}{\partial t} \\ \dfrac{\partial^2 v_2(x,t)}{\partial x^2} = r(c+c_c)\dfrac{\partial v_2(x,t)}{\partial t} - rc_c\dfrac{\partial v_1(x,t)}{\partial t} \end{cases}, \quad (3)$$

where $n = 1$ and $n = 2$ hold in the two-line and three-line systems, respectively. (3) can be rewritten as follows;

$$\begin{cases} \dfrac{\partial^2 v_1(x,t)}{\partial x^2} = rc\left\{(n\eta+1)\dfrac{\partial v_1(x,t)}{\partial t} - n\eta\dfrac{\partial v_2(x,t)}{\partial t}\right\} \\ \dfrac{\partial^2 v_2(x,t)}{\partial x^2} = rc\left\{(\eta+1)\dfrac{\partial v_2(x,t)}{\partial t} - \eta\dfrac{\partial v_1(x,t)}{\partial t}\right\} \end{cases}, \quad (4)$$

where $\eta = c_c/c$. With a linear transformation, (4) turns out to the following equation set;

$$\begin{cases} \dfrac{\partial^2 \{v_1(x,t)+nv_2(x,t)\}}{\partial x^2} = rc\dfrac{\partial \{v_1(x,t)+nv_2(x,t)\}}{\partial t} \\ \dfrac{\partial^2 \{v_1(x,t)-v_2(x,t)\}}{\partial x^2} = rc\dfrac{\partial \{v_1(x,t)-v_2(x,t)\}}{\partial (t/p)} \end{cases}, \quad (5)$$

where $p = (n+1)\eta + 1$. $v_1 + nv_2$ and $v_1 - v_2$ are called a fast and slow wave, respectively.

3. Same-Direction Drive

In this section, the case that adjacent lines are driven from the same direction is treated as illustrated in Fig. 3. As the boundary conditions, we account for an equivalent resistance of a driver MOSFET, R_t, an equivalent junction capacitance of the driver MOSFET at the drain, C_j, and an equivalent capacitance of a receiver MOSFET, C_t, as follows;

$$\begin{cases} -\dfrac{1}{r}\cdot\dfrac{\partial v_1(x,t)}{\partial x}\Big|_{x=0} = \dfrac{E_1 - v_1(0,t)}{R_t} - C_j\dfrac{\partial v_1(0,t)}{\partial t} \\ -\dfrac{1}{r}\cdot\dfrac{\partial v_1(x,t)}{\partial x}\Big|_{x=l} = C_t\dfrac{\partial v_1(l,t)}{\partial t} \\ -\dfrac{1}{r}\cdot\dfrac{\partial v_2(x,t)}{\partial x}\Big|_{x=0} = \dfrac{E_2 - v_2(0,t)}{R_t} - C_j\dfrac{\partial v_2(0,t)}{\partial t} \\ -\dfrac{1}{r}\cdot\dfrac{\partial v_2(x,t)}{\partial x}\Big|_{x=l} = C_t\dfrac{\partial v_2(l,t)}{\partial t} \end{cases}, \quad (6)$$

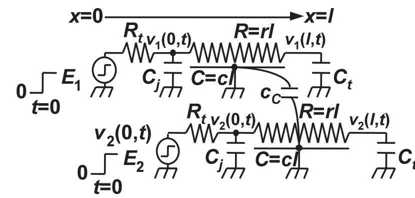

Fig. 3 Same-direction drive. Driving points are at the same end.

where E_i (i=1, 2) is a step voltage at the driving point of the line i. l is a line length. Then, we introduce the concept of the fast and slow wave mentioned in Sect. 2. (5) is replaced as follows;

$$\begin{cases} \dfrac{\partial^2 v_{fast}(x,t)}{\partial x^2} = rc\dfrac{\partial v_{fast}(x,t)}{\partial t} \\ \dfrac{\partial^2 v_{slow}(x,t)}{\partial x^2} = rc\dfrac{\partial v_{slow}(x,t)}{\partial (t/p)} \end{cases}, \quad (7)$$

where $v_{fast} = v_1 + nv_2$ and $v_{slow} = v_1 - v_2$. The boundary conditions, (6), can be replaced as well;

$$\begin{cases} -\dfrac{1}{r}\cdot\dfrac{\partial v_{fast}(x,t)}{\partial x}\Big|_{x=0} = \dfrac{(E_1+nE_2) - v_{fast}(0,t)}{R_t} \\ \qquad\qquad -C_j\dfrac{\partial v_{fast}(0,t)}{\partial t} \\ -\dfrac{1}{r}\cdot\dfrac{\partial v_{fast}(x,t)}{\partial x}\Big|_{x=l} = C_t\dfrac{\partial v_{fast}(l,t)}{\partial t} \\ -\dfrac{1}{r}\cdot\dfrac{\partial v_{slow}(x,t)}{\partial x}\Big|_{x=0} = \dfrac{(E_1-E_2) - v_{slow}(0,t)}{R_t} \\ \qquad\qquad -\dfrac{C_j}{p}\cdot\dfrac{\partial v_{slow}(0,t)}{\partial (t/p)} \\ -\dfrac{1}{r}\cdot\dfrac{\partial v_{slow}(x,t)}{\partial x}\Big|_{x=l} = \dfrac{C_t}{p}\cdot\dfrac{\partial v_{slow}(l,t)}{\partial (t/p)} \end{cases}. \quad (8)$$

On the other hand, in a single distributed RC line in Fig. 4(a), it is well known that the telegraph equation, (9), with the boundary conditions, (10), has the approximate solution, (11), at the receiving end [10];

$$\frac{\partial^2 v(x,t)}{\partial x^2} = rc\frac{\partial v(x,t)}{\partial t}, \quad (9)$$

$$\begin{cases} -\dfrac{1}{r}\cdot\dfrac{\partial v(x,t)}{\partial x}\Big|_{x=0} = \dfrac{E - v(0,t)}{R_t} \\ -\dfrac{1}{r}\cdot\dfrac{\partial v(x,t)}{\partial x}\Big|_{x=l} = C_t\dfrac{\partial v(l,t)}{\partial t} \end{cases}, \quad (10)$$

$$\begin{aligned} v(l,t) &= E\left(1 - \exp\left[-\frac{t/(RC) - 0.1}{\tau_{ElmoreWithoutCj} - 0.1}\right]\right) \\ &= E\left(1 - \exp\left[-\frac{t/(RC) - 0.1}{R_TC_T + R_T + C_T + 0.4}\right]\right) \\ &\quad \text{(if } t/(RC) > 0.1\text{)} \\ &= 0 \quad \text{(if } t/(RC) \le 0.1\text{)}, \end{aligned} \quad (11)$$

where $R = rl$, $C = cl$, $R_T = R_t/R$, and $C_T = C_t/C$. Namely, R and C are the total resistance and capacitance of the line. $\tau_{ElmoreWithoutCj}$ is the Elmore delay [11] of the line without C_j, and is $R_TC_T + R_T + C_T$+0.5. As shown in Fig. 4(b), if C_j is considered, the Elmore delay is replaced as $\tau_{ElmoreWithCj} =$

$R_T(C_T + C_J) + R_T + C_T + 0.5$, and thus (11) is rewritten as follows;

$$\begin{aligned} v(l,t) &= E\left(1 - \exp\left[-\frac{t/(RC) - 0.1}{\tau_{ElmoreWithCj} - 0.1}\right]\right) \\ &= E\left(1-\exp\left[-\frac{t/(RC)-0.1}{R_T(C_T+C_J)+R_T+C_T+0.4}\right]\right) \\ &\quad (\text{if } t/(RC) > 0.1) \\ &= 0 \quad (\text{if } t/(RC) \leq 0.1), \end{aligned} \tag{12}$$

where $C_J = C_j/C$. (12) is a solution to the single distributed RC line with C_j, and can be extended to the fast and slow waves. Based on the boundary conditions, (8), we make $E \to E_1 + nE_2$ for v_{fast}, and $E \to E_1 - E_2$, $t \to t/p$, $C_T \to C_T/p$, $C_J \to C_J/p$ for v_{slow} to obtain the following solutions;

$$\begin{cases} v_{fast}(l,t) = (E_1+nE_2) \\ \quad \cdot\left(1-\exp\left[-\frac{t/(RC) - 0.1}{R_T(C_T + C_J) + R_T + C_T + 0.4}\right]\right) \\ \quad (\text{if } t/(RC) > 0.1) \\ \quad = 0 \quad (\text{if } t/(RC) \leq 0.1) \\ v_{slow}(l,t) = (E_1-E_2) \\ \quad \cdot\left(1-\exp\left[-\frac{t/(pRC) - 0.1}{R_T(C_T+C_J)/p+R_T+C_T/p+0.4}\right]\right) \\ \quad = (E_1-E_2) \\ \quad \cdot\left(1-\exp\left[-\frac{t/(RC) - 0.1p}{R_T(C_T+C_J)+pR_T+C_T+0.4p}\right]\right) \\ \quad (\text{if } t/(RC) > 0.1p) \\ \quad = 0 \quad (\text{if } t/(RC) \leq 0.1p) \end{cases} \tag{13}$$

Since $v_{fast} = v_1 + nv_2$ and $v_{slow} = v_1 - v_2$, v_1 and v_2 are expressed with the linear combination as follows;

$$\begin{cases} v_1(l,t) = \left\{v_{fast}(l,t) + nv_{slow}(l,t)\right\}/(n+1) \\ v_2(l,t) = \left\{v_{fast}(l,t) - v_{slow}(l,t)\right\}/(n+1) \end{cases}. \tag{14}$$

Finally, the following expression for v_1 holds;

$$\begin{aligned} &v_1(l,t) \\ &= E_1-\frac{1}{n+1}\left\{(E_1+nE_2)\exp\left[-\frac{t/(RC)-0.1}{R_T(C_T+C_J)+R_T+C_T+0.4}\right]\right. \\ &\quad \left. + n(E_1-E_2)\exp\left[-\frac{t/(RC)-0.1p}{R_T(C_T+C_J)+pR_T+C_T+0.4p}\right]\right\} \\ &\quad (\text{if } t/(RC) > 0.1p) \\ &= \frac{E_1+nE_2}{n+1}\left(1-\exp\left[-\frac{t/(RC)-0.1}{R_T(C_T+C_J)+R_T+C_T+0.4}\right]\right) \\ &\quad (\text{if } 0.1 < t/(RC) \leq 0.1p) \\ &= 0 \quad (\text{if } t/(RC) \leq 0.1). \end{aligned} \tag{15}$$

Since we assume that the line 1 is a victim and the line 2 is an aggressor in this paper, we will focus on v_1 but not v_2. To verify the validity of (15) and other expressions described later on, we compare them to HSPICE simulations. Note that all HSPICE simulations in this paper are carried out using a 10-stage π-type RC model instead of a distributed RC line model. We prepare the following parameter sets for wide-range comparison in terms of η, R_T, C_T, and C_J;

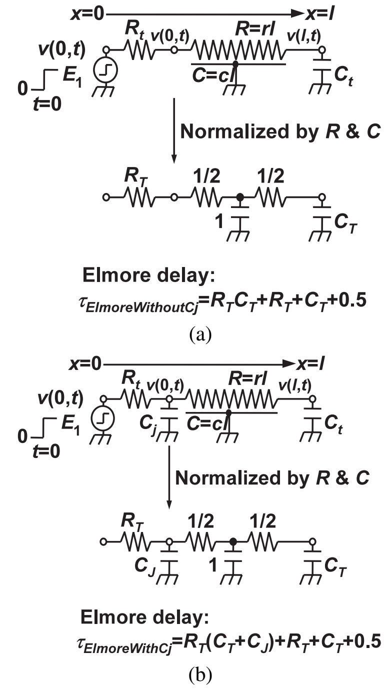

Fig. 4 Boundary conditions and Elmore delays for distributed RC lines (a) without C_j and (b) with C_j.

- $\eta \to \{0, 0.1, 0.2, 0.5, 1, 2, 5, 10\}$.
- $R_T \to \{0, 0.1, 0.2, 0.5, 1, 2, 5, 10\}$.
- $C_T \to \{0, 0.1, 0.2, 0.5, 1, 2, 5, 10\}$.
- $C_J \to \{0, 0.1, 0.2, 0.5, 1, 2, 5, 10\}$.

That is, the number of combinations is 4,096 (= $8\times8\times8\times8$).

Unfortunately, since (15) is originally derived from the approximate solution, (11), and besides the Elmore delay, $\tau_{ElmoreWithCj}$, is assumed in (12), (15) does not fit to the HSPICE simulations very much, particularly, at a large value of C_J. For instance, the relative delay error in (15) reaches 14.6% when $\eta = 0$, $R_T = 0.1$, $C_T = 0.5$, and $C_J = 10$ even though η is zero and there is no coupling effect. To suppress the relative error down to 10%, we introduce a fitting technique with MATLAB Optimization Toolbox [12], and put fitting terms to (15). (15) is rewritten as follows;

$$\begin{aligned} &v_1(l,t) \\ &= E_1-\frac{1}{n+1}\left\{(E_1+nE_2)\exp\left[-\frac{t/(RC)-0.1-a_1\sqrt{R_TC_J}}{R_T(C_T+a_2C_J)+R_T+C_T+0.4}\right]\right. \\ &\quad \left. + n(E_1-E_2)\exp\left[-\frac{t/(RC)-0.1p-a_1\sqrt{R_TC_J}}{R_T(C_T+a_2C_J)+pR_T+C_T+0.4p}\right]\right\} \end{aligned}$$

$$
\begin{aligned}
&\quad (\text{if } t/(RC) > 0.1p + a_1\sqrt{R_T C_J}) \\
&= \frac{E_1+nE_2}{n+1}\left(1-\exp\left[-\frac{t/(RC)-0.1-a_1\sqrt{R_T C_J}}{R_T(C_T+a_2C_J)+R_T+C_T+0.4}\right]\right) \\
&\quad (\text{if } 0.1 + a_1\sqrt{R_T C_J} < t/(RC) \le 0.1p + a_1\sqrt{R_T C_J}) \\
&= 0 \quad (\text{if } t/(RC) \le 0.1 + a_1\sqrt{R_T C_J}), \qquad (16)
\end{aligned}
$$

where a_1 and a_2 are fitting parameters. The fitting terms are inserted so that (16) becomes (15) when C_J=0 (see Appendix A.1 for more detail).

3.1 Crosstalk Noise Amplitude

In the crosstalk noise estimation, we substitute $E_1 \to 0$ and $E_2 \to E$ in (16) as follows;

$$
\begin{aligned}
\frac{v_1(l,t)}{E} &= -\frac{n}{n+1}\left(\exp\left[-\frac{t/(RC)-0.1-a_1\sqrt{R_T C_J}}{\tau_{fast}}\right]\right. \\
&\qquad \left.-\exp\left[\frac{t/(RC)-0.1p-a_1\sqrt{R_T C_J}}{\tau_{slow}}\right]\right) \\
&\qquad (\text{if } t/(RC) > 0.1p + a_1\sqrt{R_T C_J}) \\
&= \frac{n}{n+1}\left(1-\exp\left[-\frac{t/(RC)-0.1-a_1\sqrt{R_T C_J}}{\tau_{fast}}\right]\right) \\
&\qquad (\text{if } 0.1 + a_1\sqrt{R_T C_J} < t/(RC) \\
&\qquad\quad \le 0.1p + a_1\sqrt{R_T C_J}) \\
&= 0 \quad (\text{if } t/(RC) \le 0.1 + a_1\sqrt{R_T C_J}), \qquad (17)
\end{aligned}
$$

where $\tau_{fast} = R_T(C_T + a_2C_J) + R_T + C_T + 0.4$ and $\tau_{slow} = R_T(C_T + a_2C_J) + pR_T + C_T + 0.4p$. The crosstalk noise comparison between (17) and the HSPICE simulations are shown in Fig. 5 when $n = 2$, $\eta = 1$, and $R_T = C_T = C_J = 0$, where the noise peak in the HSPICE simulation is $0.4E$. This means that the noise induced by the crosstalk goes up to 40% of the signal swing on this condition, which often happens in VLSI designs and may cause malfunction, particularly, in dynamic circuits.

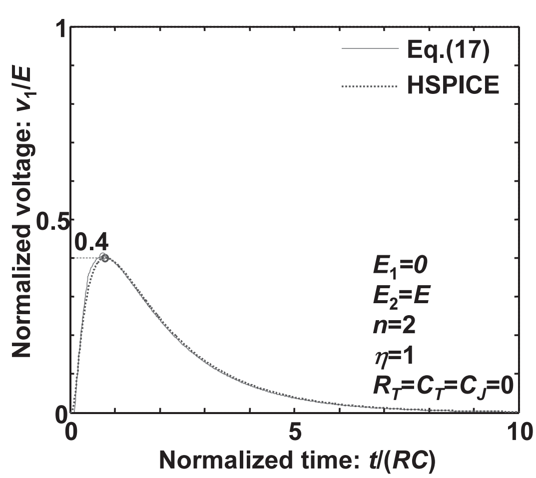

Fig. 5 Crosstalk noise comparison between (17) and HSPICE simulation (same-direction drive).

By differentiating (17) and solving $\partial v_1/\partial t$=0 in terms of t, we can obtain the time to give the noise peak, $t_{p,same}$, and then can find the noise peak itself. However, since (17) is monotone increasing function when $t/(RC) \le 0.1p + a_1\sqrt{R_T C_J}$, $t_{p,same}/(RC) \ge 0.1p + a_1\sqrt{R_T C_J}$ must hold. In this paper, if the obtained $t_{p,same}/(RC)$ is less than $0.1p + a_1\sqrt{R_T C_J}$, we replace $t_{p,same}/(RC)$ to $0.1p + a_1\sqrt{R_T C_J}$ as follows;

$$
\begin{aligned}
\frac{t_{p,same}}{RC} &= \frac{\tau_{fast}\tau_{slow}\ln[\tau_{fast}/\tau_{slow}] + 0.1(p\tau_{fast}-\tau_{slow})}{\tau_{fast}-\tau_{slow}} \\
&\qquad + a_1\sqrt{R_T C_J} \\
&\left(\text{if } \frac{\tau_{fast}\tau_{slow}\ln[\tau_{fast}/\tau_{slow}] + 0.1(p\tau_{fast}-\tau_{slow})}{\tau_{fast}-\tau_{slow}} \ge 0.1p\right) \\
&= 0.1p + a_1\sqrt{R_T C_J} \\
&\left(\text{if } \frac{\tau_{fast}\tau_{slow}\ln[\tau_{fast}/\tau_{slow}] + 0.1(p\tau_{fast}-\tau_{slow})}{\tau_{fast}-\tau_{slow}} < 0.1p\right). \qquad (18)
\end{aligned}
$$

By putting (18) back to (17), the noise peak, $v_{p,same}$, is obtained as follows;

$$
\begin{aligned}
\frac{v_{p,same}}{E} &= -\frac{n}{n+1}\left(\exp\left[-\frac{\tau_{slow}\ln[\tau_{fast}/\tau_{slow}]+0.1(p-1)}{\tau_{fast}-\tau_{slow}}\right]\right. \\
&\qquad \left.-\exp\left[-\frac{\tau_{fast}\ln[\tau_{fast}/\tau_{slow}]+0.1(p-1)}{\tau_{fast}-\tau_{slow}}\right]\right) \\
&\left(\text{if } \frac{\tau_{fast}\tau_{slow}\ln[\tau_{fast}/\tau_{slow}] + 0.1(p\tau_{fast}-\tau_{slow})}{\tau_{fast}-\tau_{slow}} \ge 0.1p\right) \\
&= -\frac{n}{n+1}\left\{\exp\left[-\frac{0.1(p-1)}{\tau_{fast}}\right]-1\right\} \\
&\left(\text{if } \frac{\tau_{fast}\tau_{slow}\ln[\tau_{fast}/\tau_{slow}] + 0.1(p\tau_{fast}-\tau_{slow})}{\tau_{fast}-\tau_{slow}} < 0.1p\right). \qquad (19)
\end{aligned}
$$

(19) does not include the fitting parameter a_1 but a_2. For $v_{p,same}$, since a_2=0.70 makes the absolute error least in the both cases that n=1 and n=2, we set $\tau_{fast} = R_T(C_T + 0.70C_J) + R_T + C_T + 0.4$ and $\tau_{slow} = R_T(C_T + 0.70C_J) + pR_T + C_T + 0.4p$ in this crosstalk noise estimation. For $t_{p,same}$, a_1=0 is optimum, and thus (18) can be rewritten as follows;

$$
\begin{aligned}
\frac{t_{p,same}}{RC} &= \frac{\tau_{fast}\tau_{slow}\ln[\tau_{fast}/\tau_{slow}] + 0.1(p\tau_{fast}-\tau_{slow})}{\tau_{fast}-\tau_{slow}} \\
&\left(\text{if } \frac{\tau_{fast}\tau_{slow}\ln[\tau_{fast}/\tau_{slow}] + 0.1(p\tau_{fast}-\tau_{slow})}{\tau_{fast}-\tau_{slow}} \ge 0.1p\right) \\
&= 0.1p \\
&\left(\text{if } \frac{\tau_{fast}\tau_{slow}\ln[\tau_{fast}/\tau_{slow}] + 0.1(p\tau_{fast}-\tau_{slow})}{\tau_{fast}-\tau_{slow}} < 0.1p\right). \qquad (20)
\end{aligned}
$$

3.1.1 Case that $n = 1$ (two-line system)

The relative error of $t_{p,same}$ in (20) is as much as 55.4% when

η = 0.1, R_T=0.5, C_T=0, and C_J=10, while the absolute error of $v_{p,same}$ in (19) is 0.033E (3.3%) as shown in Fig. 6 when η = 5, R_T=0.1, C_T=1, and C_J=10. Note that the value is an absolute error.

To minimize a relative error in a crosstalk noise amplitude, a_2 = 0.78 is better fitting than a_2 = 0.70. The relative error of $v_{p,same}$ in (19) is 24.0% ((19) = 3.48×10^{-3} and HSPICE = 4.32×10^{-3}) when η = 0.1, R_T=10, C_T=0, and C_J=10. Like this, a small absolute error results in a large relative error since the crosstalk noise amplitude sometimes becomes zero or a very small value. Table 1 is an error table at various values of $v_{p,same}$, in which the relative error turns out smaller as the noise amplitude is increased.

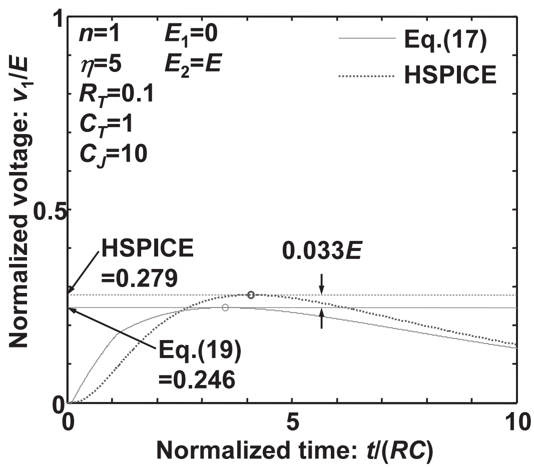

Fig. 6 Worst-case absolute error in crosstalk noise amplitude (n=1, same-direction drive).

Table 1 Relative errors of (19) when n=1. [ ] signify an absolute error.

$v_{p,same}$	≥0	≥0.1E	≥0.2E	≥0.3E	≥0.4E
Error	24.0% [0.033E]	19.0% [0.033E]	15.6% [0.033E]	12.1% [0.032E]	5.8% [0.025E]

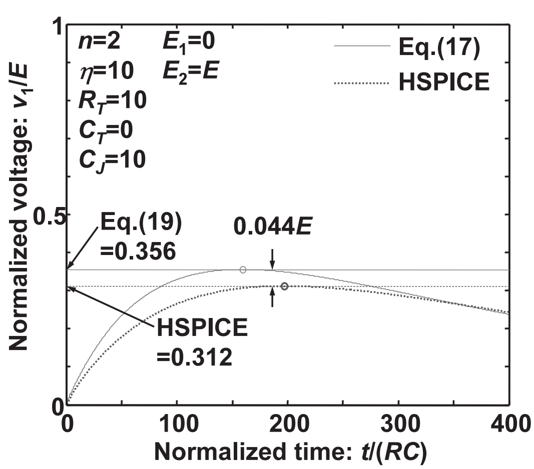

Fig. 7 Worst-case absolute error in crosstalk noise amplitude (n=2, same-direction drive).

3.1.2 Case that n = 2 (two-line system)

The absolute error of $v_{p,same}$ is 0.044E (4.4%) as depicted in Fig. 7 when a_2=0.70, η = 10, R_T=10, C_T=0, and C_J=10, although the worst-case relative error of $t_{p,same}$ is as much as 56.8% when η = 10, R_T=0, C_T=0, and C_J=10.

The relative error of $v_{p,same}$ is 23.9% ((19) = 6.93×10^{-3} and HSPICE = 8.59×10^{-3}) when a_2=0.78, η = 0.1, R_T=10, C_T=0, and C_J=10. Table 2 is an error table when $v_{p,same}$ is varied.

3.2 Delay

As expressed in (16), v_1 depends on values of E_1 and E_2. In the delay estimation of the line 1, although we make $E_1 \to E$, E_2 has three cases;

- $E_2 \to E$ indicates an in-phase drive, where the adjacent lines are driven in phase. In this case, $v_1(x,t) = v_2(x,t)$ holds at any position at any time because $E_1 = E_2 = E$, which means that no current flows between a coupling capacitor and the coupling capacitance can be canceled out even if there is some capacitance between the lines. This phenomenon can be explained as a kind of the Mirror Effect that makes $c_c = 0$, and thus $\eta = 0$ represents the in-phase drive by definition.
- When $E_2 \to 0$, we call it an $E_2 = 0$ drive, where the line 1 is only driven and the line 2 is not.
- The last case that $E_2 \to -E$ is an out-of-phase drive, where the adjacent lines are driven out of phase.

The delay comparisons between (16) and the HSPICE simulations in the three cases are shown in Fig. 8 when n = 2, η = 1, and $R_T = C_T = C_J = 0$. η = 1 means that a coupling capacitance is equal to a grounding capacitance, which often happens in VLSI designs. The figure shows that the delays in the same-direction drive case fluctuate from 0.38RC to 1.98RC according to the E_2 drives, and the out-of-phase drive has the worst-case delay. In this paper, the worst-case delay is discussed as a line delay (on the best-case delay, see Appendix A.3).

As the worst-case delay, we substitute $E_1 \to E$ and $E_2 \to -E$ in (16), but this equation does not have a positive value when $t/(RC) \leq 0.1p + a_1\sqrt{R_T C_J}$ in the case of the out-of-phase drive. Hence, the region in which $t/(RC) > 0.1p + a_1\sqrt{R_T C_J}$ is only to be considered in the delay estimation, where (16) is rewritten as follows;

Table 2 Relative errors of (19) when n=2. [ ] signify an absolute error.

$v_{p,same}$	≥0	≥0.1E	≥0.2E	≥0.3E	≥0.4E	≥0.5E	≥0.6E
Error	23.9% [0.044E]	19.6% [0.044E]	17.8% [0.044E]	14.9% [0.044E]	11.3% [0.044E]	8.1% [0.035E]	5.6% [0.035E]

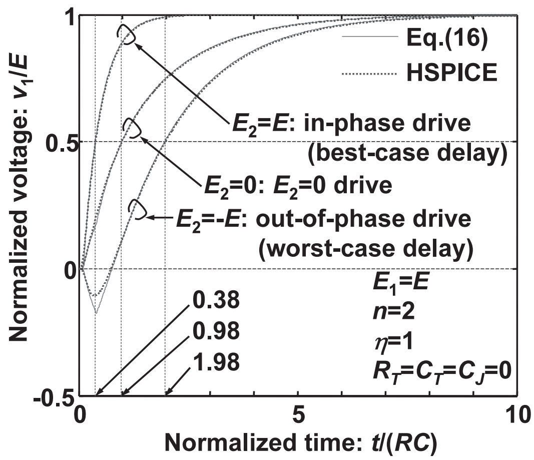

Fig. 8 Delay comparisons between (16) and HSPICE simulations (same-direction drive).

$$\frac{v_1(l,t)}{E} = 1-\frac{1}{n+1}\left\{(1-n)\exp\left[-\frac{t/(RC)-0.1-a_1\sqrt{R_TC_J}}{R_T(C_T+a_2C_J)+R_T+C_T+0.4}\right] + 2n\exp\left[-\frac{t/(RC)-0.1p-a_1\sqrt{R_TC_J}}{R_T(C_T+a_2C_J)+pR_T+C_T+0.4p}\right]\right\}$$
$$(\text{if } t/(RC) \geq 0.1p + a_1\sqrt{R_TC_J}). \tag{21}$$

Then, to find the line delay, $t_{pd,same}$, $v_1(l,t)/E$ in (21) is set to 1/2, and we need to solve the following equation in terms of $t_{pd,same}$;

$$\frac{1}{n+1}\left\{(1-n)\exp\left[-\frac{t_{pd,same}/(RC)-0.1-a_1\sqrt{R_TC_J}}{R_T(C_T+a_2C_J)+R_T+C_T+0.4}\right] + 2n\exp\left[-\frac{t_{pd,same}/(RC)-0.1p-a_1\sqrt{R_TC_J}}{R_T(C_T+a_2C_J)+pR_T+C_T+0.4p}\right]\right\} = \frac{1}{2}. \tag{22}$$

3.2.1 Case that n=1 (two-line system)

$t_{pd,same}$ in (22) is easily solved if n=1 as follows;

$$t_{pd,same}/(RC) = 0.1p+a_1\sqrt{R_TC_J}+\ln[2]\{R_T(C_T+a_2C_J) + pR_T + C_T + 0.4p\}. \tag{23}$$

Compared with the HSPICE simulations, a_1=0.19, and a_2=1 are optimum in (23), where the relative error is 6.9%. Thus, $t_{pd,same}$ finally becomes as follows;

$$t_{pd,same}/(RC) = 0.1(2\eta+1) + 0.19\sqrt{R_TC_J} + \ln[2]\{R_T(C_T+C_J) + (2\eta+1)R_T + C_T + 0.4(2\eta+1)\}$$
$$(\because p = (n+1)\eta + 1 = 2\eta + 1). \tag{24}$$

The worst-case relative error happens when $\eta = 0$, $R_T = 0.5$, C_T=0, and C_J=10 as depicted in Fig. 9.

3.2.2 Case that $n = 2$ (three-line system)

If $n = 2$, (22) becomes a sum of two exponential functions and can be represented as the following function, f;

$$f(\hat{t}) = k_{fast}\exp[-\hat{t}/\tau_{fast}] + k_{slow}\exp[-\hat{t}/\tau_{slow}], \tag{25}$$

where

$$\begin{cases} \hat{t} = t_{pd,same}/(RC) \\ p = (n+1)\eta + 1 = 3\eta + 1 \\ \tau_{fast} = R_T(C_T + a_2C_J) + R_T + C_T + 0.4 \\ \tau_{slow} = R_T(C_T + a_2C_J) + pR_T + C_T + 0.4p \\ k_{fast} = -\dfrac{1}{3}\exp\left[\dfrac{0.1 + a_1\sqrt{R_TC_J}}{\tau_{fast}}\right] \\ k_{slow} = \dfrac{4}{3}\exp\left[\dfrac{0.1p + a_1\sqrt{R_TC_J}}{\tau_{slow}}\right] \end{cases}. \tag{26}$$

Then, we assume that (25) is approximate to the following single exponential function, g;

$$g(\hat{t}) = k_{same}\exp[-\hat{t}/\tau_{same}]. \tag{27}$$

Here, we introduce the moment matching method [13] using (25) and (27) as follows;

$$\begin{cases} m_0 = k_{fast} + k_{slow} \Leftrightarrow n_0 = k_{same} \\ m_1 = \displaystyle\int_0^\infty f(\hat{t})d\hat{t} = k_{fast}\tau_{fast} + k_{slow}\tau_{slow} \\ \quad\Leftrightarrow n_1 = \displaystyle\int_0^\infty g(\hat{t})d\hat{t} = k_{same}\tau_{same} \\ m_2 = \displaystyle\int_0^\infty \hat{t}f(\hat{t})d\hat{t} = k_{fast}\tau_{fast}^2 + k_{slow}\tau_{slow}^2 \\ \quad\Leftrightarrow n_2 = \displaystyle\int_0^\infty \hat{t}g(\hat{t})d\hat{t} = k_{same}\tau_{same}^2 \\ \quad\vdots \\ m_j = \displaystyle\int_0^\infty \hat{t}^{j-1}f(\hat{t})d\hat{t} = k_{fast}\tau_{fast}^j + k_{slow}\tau_{slow}^j \\ \quad\Leftrightarrow n_j = \displaystyle\int_0^\infty \hat{t}^{j-1}g(\hat{t})d\hat{t} = k_{same}\tau_{same}^j \\ m_{j+1} = \displaystyle\int_0^\infty \hat{t}^j f(\hat{t})d\hat{t} = k_{fast}\tau_{fast}^{j+1} + k_{slow}\tau_{slow}^{j+1} \\ \quad\Leftrightarrow n_{j+1} = \displaystyle\int_0^\infty \hat{t}^j g(\hat{t})d\hat{t} = k_{same}\tau_{same}^{j+1} \\ \quad\vdots \end{cases}, \tag{28}$$

where m_i and n_i ($i = 0, 1, 2, \ldots, j, j+1, \ldots$) are the i-th order moments of f and g, respectively, and we assume $m_i = n_i$ based on the moment matching method. Once we obtain m_j and m_{j+1}, τ_{same} and k_{same} are given as follows;

$$\begin{cases} \tau_{same} = m_{j+1}/m_j \\ k_{same} = m_j^{j+1}/m_{j+1}^j \end{cases}. \tag{29}$$

Then, $\hat{t}$ can be reached as follows;

$$\hat{t} = \tau_{same}\ln[2k_{same}] = \frac{m_{j+1}}{m_j}\ln\left[\frac{2\,m_j^{j+1}}{m_{j+1}^j}\right]$$
$$(\because k_{same}\exp[-\hat{t}/\tau_{same}] = 1/2), \tag{30}$$

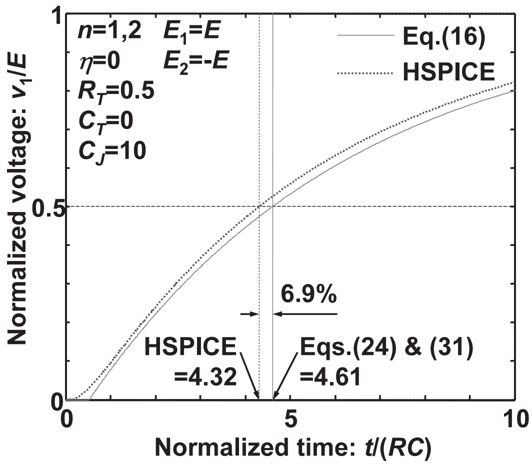

Fig. 9 Worst-case relative error in delay (same-direction drive).

where j is a fitting parameter. Again by being compared with the HSPICE simulations, a_1=0.19, a_2=1, and j=2, are obtained as the optimum condition. Therefore, (30) can be rewritten as follows;

$$\frac{t_{pd,same}}{RC} = \frac{m_3}{m_2} \ln\left[\frac{2\,m_2^3}{m_3^2}\right], \tag{31}$$

where

$$\begin{cases} \tau_{fast} = R_T(C_T + C_J) + R_T + C_T + 0.4 \\ \tau_{slow} = R_T(C_T + C_J) + (3\eta+1)R_T + C_T + 0.4(3\eta+1) \\ k_{fast} = -\dfrac{1}{3}\exp\left[\dfrac{0.1 + 0.19\sqrt{R_T C_J}}{\tau_{fast}}\right] \\ k_{slow} = \dfrac{4}{3}\exp\left[\dfrac{0.1(3\eta+1) + 0.19\sqrt{R_T C_J}}{\tau_{slow}}\right] \\ m_2 = k_{fast}\tau_{fast}^2 + k_{slow}\tau_{slow}^2 \\ m_3 = k_{fast}\tau_{fast}^3 + k_{slow}\tau_{slow}^3 \end{cases}. \tag{32}$$

The worst-case relative error in (31) is 6.9% as well as the case that n=1 when $\eta = 0$, R_T=0.5, C_T=0, and C_J=10. On this condition, the waveforms are the same as Fig. 9.

4. Opposite-Direction Drive

In this section, the case that adjacent lines are driven from the opposite direction in Fig. 10 is handled. With the Laplace transformation, (5) is replaced in the s-domain as follows;

$$\begin{cases} \dfrac{\partial^2 \{V_1(x,s) + nV_2(x,s)\}}{\partial x^2} = rcs\{V_1(x,s) + nV_2(x,s)\} \\ \dfrac{\partial^2 \{V_1(x,s) - V_2(x,s)\}}{\partial x^2} = rcps\{V_1(x,s) - V_2(x,s)\} \end{cases}. \tag{33}$$

The solutions to (33) are expressed as follows;

$$\begin{cases} V_1(x,s) + nV_2(x,s) = K_1' e^{\sqrt{src}x} + K_2' e^{-\sqrt{src}x} \\ V_1(x,s) - V_2(x,s) = K_3' e^{\sqrt{srcp}x} + K_4' e^{-\sqrt{srcp}x} \end{cases}, \tag{34}$$

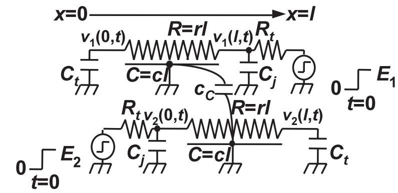

Fig. 10 Opposite-direction drive. Driving points are on the opposite sides.

where K_1', K_2', K_3', and K_4' are integration constants. With linear combination, (34) is rewritten as follows;

$$\begin{cases} (n+1)V_1(x,s) = \left(K_1' e^{\sqrt{src}x} + K_2' e^{-\sqrt{src}x}\right) \\ \quad +n\left(K_3' e^{\sqrt{srcp}x} + K_4' e^{-\sqrt{srcp}x}\right) \\ (n+1)V_2(x,s) = \left(K_1' e^{\sqrt{src}x} + K_2' e^{-\sqrt{src}x}\right) \\ \quad -\left(K_3' e^{\sqrt{srcp}x} + K_4' e^{-\sqrt{srcp}x}\right) \end{cases}. \tag{35}$$

Finally, the following expressions are the general solutions to (33) in the s-domain;

$$\begin{cases} V_1(x,s) = K_1 e^{\sqrt{src}x} + K_2 e^{-\sqrt{src}x} + nK_3 e^{\sqrt{srcp}x} \\ \quad + nK_4 e^{-\sqrt{srcp}x} \\ V_2(x,s) = K_1 e^{\sqrt{src}x} + K_2 e^{-\sqrt{src}x} - K_3 e^{\sqrt{srcp}x} \\ \quad - K_4 e^{-\sqrt{srcp}x} \end{cases}, \tag{36}$$

where the integration constants, K_1, K_2, K_3, and K_4 are to be taken from boundary conditions, which in the t-domain are as follows;

$$\begin{cases} -\dfrac{1}{r}\cdot\left.\dfrac{\partial v_1(x,t)}{\partial x}\right|_{x=0} = -C_t\dfrac{\partial v_1(0,t)}{\partial t} \\ -\dfrac{1}{r}\cdot\left.\dfrac{\partial v_1(x,t)}{\partial x}\right|_{x=l} = -\dfrac{E_1 - v_1(l,t)}{R_t} + C_j\dfrac{\partial v_1(l,t)}{\partial t} \\ -\dfrac{1}{r}\cdot\left.\dfrac{\partial v_2(x,t)}{\partial x}\right|_{x=0} = \dfrac{E_2 - v_2(0,t)}{R_t} - C_j\dfrac{\partial v_2(0,t)}{\partial t} \\ -\dfrac{1}{r}\cdot\left.\dfrac{\partial v_2(x,t)}{\partial x}\right|_{x=l} = C_t\dfrac{\partial v_2(l,t)}{\partial t} \end{cases}. \tag{37}$$

(37) can be replaced in the s-domain as follows.

$$\begin{cases} -\dfrac{1}{r}\cdot\left.\dfrac{\partial V_1(x,s)}{\partial x}\right|_{x=0} = -sC_tV_1(0,s) \\ -\dfrac{1}{r}\cdot\left.\dfrac{\partial V_1(x,s)}{\partial x}\right|_{x=l} = -\dfrac{E_1/s - V_1(l,s)}{R_t} + sC_jV_1(l,s) \\ -\dfrac{1}{r}\cdot\left.\dfrac{\partial V_2(x,s)}{\partial x}\right|_{x=0} = \dfrac{E_2/s - V_2(0,s)}{R_t} - sC_jV_2(0,s) \\ -\dfrac{1}{r}\cdot\left.\dfrac{\partial V_2(x,s)}{\partial x}\right|_{x=l} = sC_tV_2(l,s) \end{cases}. \tag{38}$$

4.1 Crosstalk Noise Amplitude

Unless R_t, C_t, and C_j are all zero, we cannot easily solve noise peak since analytical expressions turn out to be very complicated. The case that $R_t = C_t = C_j = 0$, however, gives the worst-case scenario in terms of the noise peak because coupling effect is mitigated if R_t, C_t, or C_j is not zero. The noise peak in the HSPICE simulation are shown in Fig. 11 when $n = 2$, $\eta = 1$, and $R_T = C_T = C_J = 0$, where the amplitude is $0.4E$ as well as the same-direction drive case.

At first, we treat the case that $R_t = C_t = C_j=0$, and extend it to a general case. The boundary conditions, (38), can be rewritten as follows when $R_t = C_t = C_j = 0$;

$$\begin{cases} \left.\dfrac{\partial V_1(x,s)}{\partial x}\right|_{x=0} = 0 \\ V_1(l,s) = E_1/s \\ V_2(0,s) = E_2/s \\ \left.\dfrac{\partial V_2(x,s)}{\partial x}\right|_{x=l} = 0 \end{cases}. \tag{39}$$

(36) with the boundary condition, (39), yields the following equation set;

$$\begin{cases} K_1\gamma_1 - K_2\gamma_1 + nK_3\gamma_2 - nK_4\gamma_2 = 0 \\ K_1 e^{\gamma_1 l} + K_2 e^{-\gamma_1 l} + nK_3 e^{\gamma_2 l} + nK_4 e^{-\gamma_2 l} = E_1/s \\ K_1 + K_2 - K_3 - K_4 = E_2/s \\ K_1\gamma_1 e^{\gamma_1 l} - K_2\gamma_1 e^{-\gamma_1 l} - K_3\gamma_2 e^{\gamma_2 l} + K_4\gamma_2 e^{-\gamma_2 l} = 0 \end{cases}, \tag{40}$$

where $\gamma_1 = \sqrt{sRC}$ and $\gamma_2 = \sqrt{spRC}$.

In noise-peak estimation, we substitute $E_1 \to 0$ and $E_2 \to E$, and solve (40) in terms of K_1, K_2, K_3, and K_4. By putting them in (36), $V_1(0,s)$ is obtained as follows;

$$\frac{V_1(0,s)}{E} = -\frac{n}{s}\frac{\begin{array}{c}(\gamma_1-\gamma_2)(n\gamma_1+\gamma_2)e^{2(\gamma_1+\gamma_2)} + K_1 e^{2\gamma_1} \\ +K_3 e^{\gamma_1+\gamma_2} + K_5 e^{2\gamma_1} + O_1(n,\gamma_1,\gamma_2)\end{array}}{\begin{array}{c}(\gamma_1+n\gamma_2)(n\gamma_1+\gamma_2)e^{2(\gamma_1+\gamma_2)} + K_2 e^{2\gamma_1} \\ +K_4 e^{\gamma_1+\gamma_2} + K_6 e^{2\gamma_1} + O_2(n,\gamma_1,\gamma_2)\end{array}}. \tag{41}$$

The noise peak, $v_{p,oppo}$, can be calculated with the following initial value theorem of the Laplace transformation because $v_{p,oppo}$ is given when $t = 0$ if $R_t = C_t = C_j = 0$;

$$\frac{v_{p,oppo}}{E} = \frac{v_1(0,+0)}{E} = \lim_{s\to\infty}\frac{sV_1(0,s)}{E} = \frac{n\sqrt{p}-n}{n\sqrt{p}+1}$$
$$(\text{exact if } R_t = C_t = C_j = 0). \tag{42}$$

Then, for a general case that R_t, C_t, or C_j is not zero, we extend (42) and introduce the fitting terms with the fitting parameters, d_1, d_2, d_3, and d_4, to it as follows;

$$\frac{v_{p,oppo}}{E} = \frac{n\sqrt{p}-n}{n\sqrt{p}+1+d_1\sqrt{C_T}+d_2\sqrt{R_T C_J}} \cdot \frac{\sqrt{R_T}+\sqrt{R_T C_T}+1}{d_3\sqrt{R_T}+d_4\sqrt{R_T C_T}+1}, \tag{43}$$

where the fitting terms are inserted so that (43) becomes (42) when $R_T = C_T = C_J = 0$ (see Appendix A.2 for more detail).

4.1.1 Case that n=1 (two-line system)

In (43), d_1=2.96, d_2=1.05, d_3=1.48, and d_4=0.81 are optimum for the least absolute error. The absolute error of $v_{p,oppo}$ is $0.078E$ (7.8%) when $\eta = 5$, R_T=10, C_T=0.1, and C_J=1 as shown in Fig. 12.

To minimize a relative error in a crosstalk noise amplitude, another fitting parameter set of d_1=3.29, d_2=2.65, d_3=1.11, and d_4=1.91 is better fitting. The relative error of $v_{p,oppo}$ is 63.8% ((43) = 21.08×10^{-3} and HSPICE = 7.64×10^{-3}) when $\eta = 0.1$, R_T=0, C_T=10, and C_J=5. The relative error becomes large due to the same reason in the same-direction drive case. Table 3 is an error table at various values of $v_{p,oppo}$.

4.1.2 Case that n=2 (three-line system)

d_1=3.99, d_2=1.81, d_3=1.14, and d_4=0.94 are optimum for the least absolute error. The absolute error of $v_{p,oppo}$ is $0.098E$(9.8%) when $\eta = 5$, R_T=10, C_T=0.2, and C_J=1 as shown in Fig. 13.

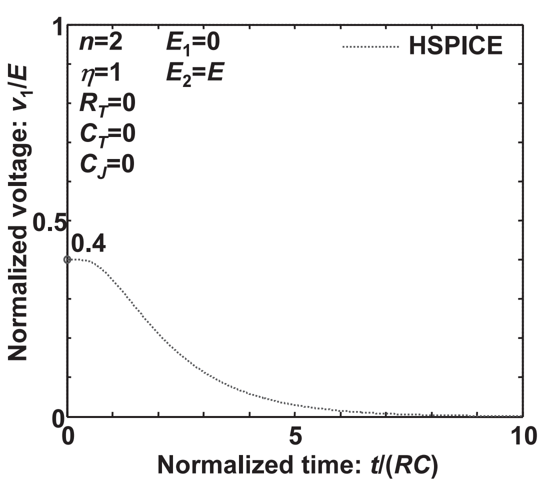

Fig. 11 Crosstalk noise in HSPICE simulation (opposite-direction drive).

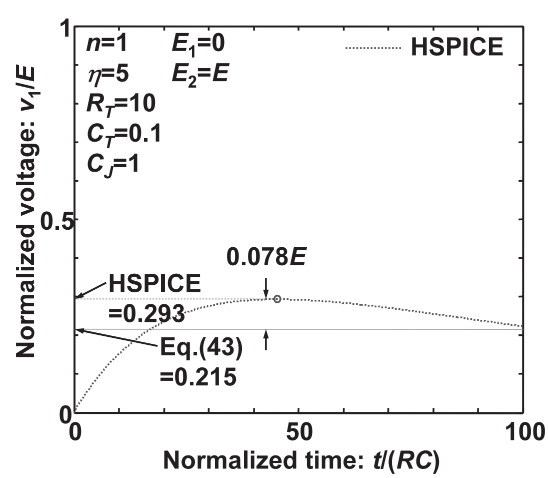

Fig. 12 Worst-case absolute error in crosstalk noise amplitude (n=1, opposite-direction drive).

Table 3 Relative errors of (43) when n=1. [ ] signify an absolute error.

$v_{p,oppo}$	≥0	≥0.1E	≥0.2E	≥0.3E	≥0.4E	≥0.5E	≥0.6E
Error	63.8% [0.078E]	63.8% [0.078E]	63.2% [0.078E]	57.7% [0.078E]	42.7% [0.076E]	23.0% [0.076E]	12.1% [0.066E]

Table 4 Relative errors of (43) when n=2. [ ] signify an absolute error.

$v_{p,oppo}$	≥0	≥0.1E	≥0.2E	≥0.3E	≥0.4E	≥0.5E	≥0.6E	≥0.7E
Error	63.3% [0.098E]	63.3% [0.098E]	63.3% [0.098E]	62.4% [0.098E]	59.8% [0.098E]	53.1% [0.097E]	29.3% [0.094E]	11.1% [0.060E]

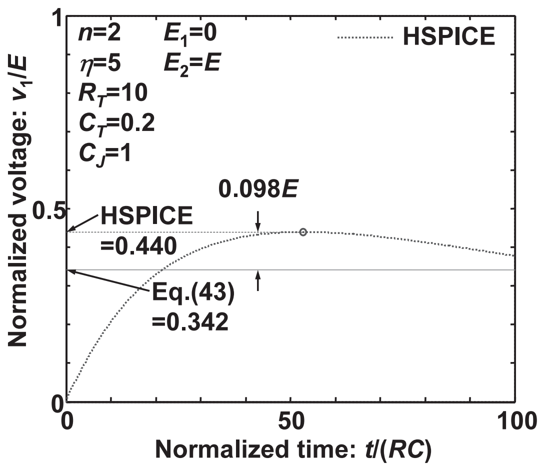

Fig. 13 Worst-case absolute error in crosstalk noise amplitude (n=2, opposite-direction drive).

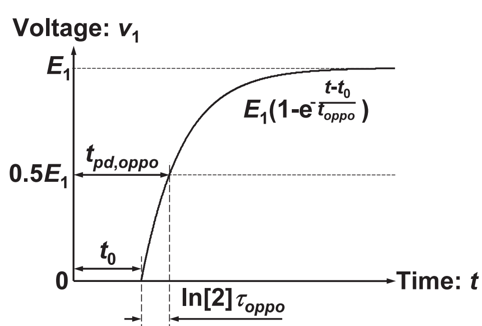

Fig. 14 Approximate voltage waveform at the receiving point.

The relative error of $v_{p,oppo}$ is 63.3% ((43) = 40.33×10^{-3} and HSPICE = 14.78×10^{-3}) when d_1=4.96, d_2=3.51, d_3=1.27, d_4=1.87, $\eta = 0.1$, R_T=0, C_T=10, and C_J=5. Table 4 is an error table when $v_{p,oppo}$ is varied.

4.2 Delay

In order to obtain a line delay, we again introduce the moment matching method [13]. As shown in Fig. 14, we assume that an approximate voltage waveform at the receiving point $v_1(0,t)$ has a form of exponential function with a time constant, τ_{oppo}, and pure delay, t_0, as follows;

$$v_1(0,t) = E_1\left(1 - \exp[-(t-t_0)/\tau_{oppo}]\right). \tag{44}$$

Then, the coefficients of the zero-th order moment, M_0, and first order moment, M_1, in the exact solution to (36) are supposed to be matched to those in the approximate voltage waveform as follows;

$$\begin{aligned} &E_1/s - s^0 M_0 + s^1 M_1 + O_{exact}\left(s^2\right) \\ &\quad\Leftrightarrow E_1/s - s^0(\tau_{oppo} + t_0) + s^1\left(\tau_{oppo}^2 + \tau_{oppo}t_0 + t_0^2/2\right) \\ &\quad\quad + O_{approx}\left(s^2\right), \end{aligned} \tag{45}$$

where the left-hand side is the Taylor expansion of V_1 in (36), and the right-hand side is that of the approximate voltage waveform in Fig. 14. Thus, the following equation set holds;

$$\begin{cases} \tau_{oppo} + t_0 = M_0 \\ \tau_{oppo}^2 + \tau_{oppo}t_0 + t_0^2/2 = M_1 \end{cases}. \tag{46}$$

The solutions to (46) are as follows;

$$\begin{cases} \tau_{oppo} = \sqrt{2M_1 - M_0^2} \\ t_0 = M_0 - \tau_{oppo} \end{cases}. \tag{47}$$

Finally, the line delay, $t_{pd,oppo}$, can be expressed as follows;

$$\begin{aligned} t_{pd,oppo} &= t_0 + \ln[2]\tau_{oppo} \\ &= M_0 - \ln[e/2]\sqrt{2M_1 - M_0^2}, \end{aligned} \tag{48}$$

where M_0 and M_1 can be obtained as follows from (36) and the boundary conditions, (38);

$$\begin{cases} M_0/(RC) = [E_1\{n\eta(2R_T+1) + 2R_TC_T \\ +2R_TC_J + 2R_T + 2C_T + 1\} - E_2n\eta(2R_T+1)]/2 \\ M_1/(RC)^2 = [E_1\{n^2\eta^2(24R_T^2 + 20R_T + 5) \\ +n\eta^2(24R_T^2 + 20R_T + 3) \\ +2n\eta(24R_T^2C_T + 24R_T^2 + 30R_TC_T + 20R_T + 10C_T + 5) \\ +24R_T^2C_T^2 + 48R_T^2C_T + 48R_TC_T^2 + 24R_T^2 + 60R_TC_T \\ +24C_T^2 + 20R_T + 20C_T + 5\} - E_2\{n^2\eta^2(24R_T^2 + 20R_T + 5) \\ +n\eta^2(24R_T^2 + 20R_T + 3) \\ +2n\eta(24R_T^2C_T + 24R_T^2 + 30R_TC_T + 20R_T \\ +8C_T + 4)\}]/24 \end{cases}. \tag{49}$$

The delay comparisons between (44) and the HSPICE simulations are shown in Fig. 15 when n=2, $\eta = 1$, and $R_T = C_T = C_J = 0$. The delays in the opposite-direction drive case fluctuate from 0.25RC to 1.90RC according to the E_2 drives, and the out-of-phase and in-phase drives have the worst-case and best-case delays, respectively. As well as the same-direction drive case, the worst-case delay is discussed as a line delay. See Appendix A.4 for the best-case delay. However, the delay accuracy in the best-case analysis is bad. As described in the previous subsection, when η is large, the crosstalk noise surges at near $E/2$ or above $E/2$, which gives a fatal influence to the best-case delay accuracy.

To obtain the worst-case delay, we substitute $E_1 \to E$ and $E_2 \to -E$, and then rewrite (49) as follows;

$$\begin{cases} M_0/(RC) = E\{2n\eta(2R_T+1)+2R_TC_T+2R_TC_J \\ \quad +2R_T+2C_T+1\}/2 \\ M_1/(RC)^2 = E\{2n^2\eta^2(24R_T^2+20R_T+5) \\ +2n\eta^2(24R_T^2+20R_T+3) \\ +2n\eta(48R_T^2C_T+48R_T^2+60R_TC_T+40R_T+18C_T+9) \\ +24R_T^2C_T^2+48R_T^2C_T+48R_TC_T^2+24R_T^2 \\ +60R_TC_T+24C_T^2+20R_T+20C_T+5\}/24 \end{cases} . \tag{50}$$

With (50), (48) is recalculated as follows;

$$\begin{aligned} t_{pd,oppo}/(RC) &= \{2n\eta(2R_T+1)+2R_TC_T+2R_TC_J \\ &+2R_T+2C_T+1\}/2-\ln[e/2]\sqrt{[}-n^2\eta^2(4R_T+1) \\ &+n\eta^2(24R_T^2+20R_T+3)+n\eta(24R_T^2C_T+24R_T^2C_J \\ &+24R_T^2+24R_TC_T+16R_T+6C_T+3) \\ &+6R_T^2C_T^2+12R_T^2C_TC_J+6R_T^2C_J^2+12R_T^2C_T \\ &+12R_T^2C_J+12R_TC_T^2+6R_T^2+12R_TC_T \\ &+6C_T^2+4R_T+4C_T+1]/\sqrt{6} \\ &\approx n\eta\left\{\frac{\ln[e/2]}{\sqrt{6}}R_TC_T+\left(2-\frac{5\ln[e/2]}{\sqrt{6}}\right)R_T+1\right. \\ &\left.-\frac{3\ln[e/2]}{2\sqrt{6}}\right\}+\left(1-\frac{2\ln[e/2]}{\sqrt{6}}\right)(R_TC_T+R_T+C_T) \\ &+R_TC_J+\frac{1}{2}-\frac{\ln[e/2]}{\sqrt{6}} \\ &= n\eta(0.13R_TC_T+1.37R_T+0.81) \\ &+0.75(R_TC_T+R_T+C_T)+R_TC_J+0.37. \end{aligned} \tag{51}$$

However, since (51) does not fit to the HSPICE simulations very much, we again introduce the fitting parameters, b_1, b_2, b_3, b_4, b_5, and b_6, as follows;

$$\begin{aligned} t_{pd,oppo}/(RC) &= n\eta(b_1R_TC_T+b_2R_T+b_3) \\ &+b_4(R_TC_T+R_T+C_T)+b_5R_TC_J+b_6. \end{aligned} \tag{52}$$

In both cases that n=1 and n=2, b_1=0, b_2=1.48, b_3=0.78, b_4=0.75, b_5=0.75, and b_6=0.40 are optimum with a relative error of 8.1%. (52) is finally rewritten as follows;

$$\begin{aligned} t_{pd,oppo}/(RC) &= n\eta(1.48R_T+0.78) \\ &+0.75(R_TC_T+R_TC_J+R_T+C_T)+0.4. \end{aligned} \tag{53}$$

The worst-case relative error in the case that n=1 happens when η=0, R_T=10, C_T=10, and C_J=0 as shown in Fig. 16. On the other hand, the worst-case relative error in the case that n=2 occurs when η=0.1, R_T=0.1, C_T=0.5, and C_J=10 as depicted in Fig. 17.

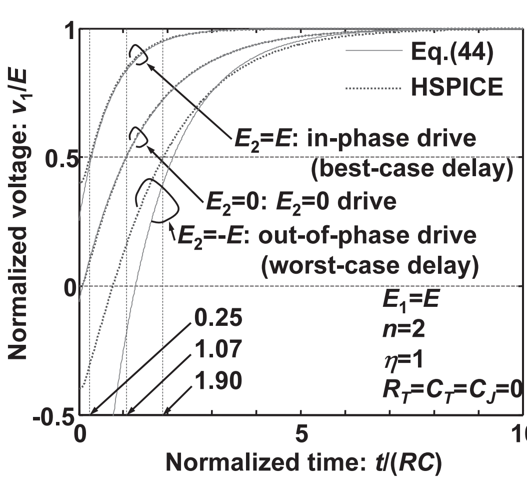

Fig. 15 Delay comparisons between (44) and HSPICE simulations (opposite-direction drive).

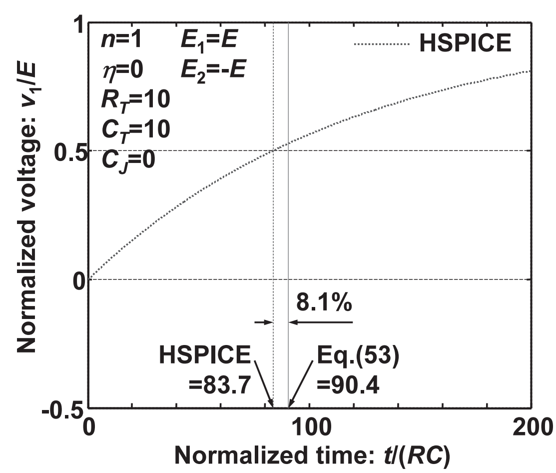

Fig. 16 Worst-case relative error in delay (n=1, opposite-direction drive).

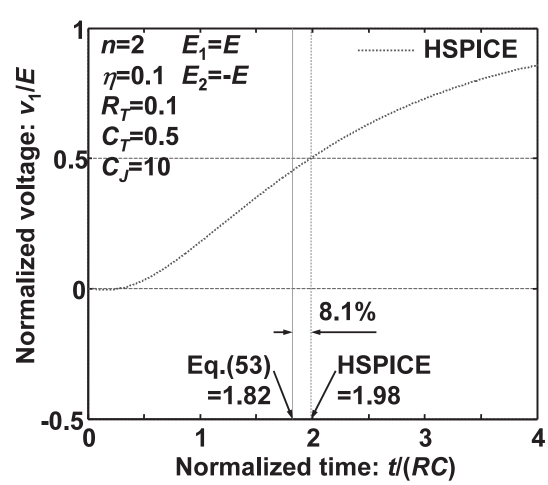

Fig. 17 Worst-case relative error in delay (n=2, opposite-direction drive).

Table 5 Expressions and relative errors at a glance. [ ] signify an absolute error.

Eq. # and relative error		Crosstalk noise amplitude		Worst-case delay	
Same-direction drive	n=1 (two lines)	(19) and $\begin{cases} \tau_{fast} = R_T(C_T + a_2 C_J) + R_T + C_T + 0.4 \\ \tau_{slow} = R_T(C_T + a_2 C_J) + pR_T + C_T + 0.4p \end{cases}$	24.0% (a_2=0.78) [0.033E (a_2=0.70)]	(24)	6.9%
	n=2 (three lines)		23.9% (a_2=0.78) [0.044E (a_2=0.70)]	(31) and (32)	
Opposite-direction drive	n=1 (two lines)	(43)	63.8% (d_1=3.29 d_2=2.65 d_3=1.11 d_4=1.91) [0.078E (d_1=2.96 d_2=1.05 d_3=1.48 d_4=0.81)]	(53)	8.1%
	n=2 (three lines)		63.3% (d_1=4.96 d_2=3.51 d_3=1.27 d_4=1.87) [0.098E (d_1=3.99 d_2=1.81 d_3=1.14 d_4=0.94)]		

5. Conclusion

The closed-form expressions for the crosstalk noise amplitude and the worst-case delay in capacitively coupled two-line and three-line systems were introduced. The both modes of the same-direction and opposite-direction drives are considered, and a junction capacitance of a driver MOSFET is also reflected. The relative and absolute errors in the crosstalk noise amplitude, and the relative error in the worst-case delay are within 63.8%, 0.098E, and 8.1%, respectively. They are useful for circuit designers to give insight to coupling related issues in an early stage of a VLSI design.

In summary, we list the expressions and relative errors in Table 5.

Acknowledgment

The authors would like to thank Dr. Shigetaka Kumashiro for useful discussion and suggestion. This study was supported in part by the semiconductor Technology Academic Research Center (STARC), Japan.

References

[1] H.B. Bakoglu, Circuits, Interconnections, and Packaging for VLSI, Addison-Wesley, 1990.

[2] A. Vittal and M. Marek-Sadowska, “Crosstalk reduction for VLSI,” IEEE Trans. Comput.-Aided Des. Integr. Circuits Syst., vol.16, no.3, pp.290–298, March 1997.

[3] A. Vittal, L.H. Chen, M. Marek-Sadowska, K.-P. Wang, and S. Yang, “Crosstalk in VLSI interconnections,” IEEE Trans. Comput.-Aided Des. Integr. Circuits Syst., vol.18, no.12, pp.1817–1824, Dec. 1999.

[4] G. Yee, R. Chandra, V. Ganesan, and C. Sechen, “Wire delay in the present of crosstalk,” Proc. ACM/IEEE International Workshop on Timing Issues in the Specification and Synthesis of Digital Systems, pp.170–175, Dec. 1997.

[5] D.S. Gao, A.T. Yang, and S.M. Kang, “Modeling and simulation of interconnection delays and crosstalks in high-speed integrated circuits,” IEEE Trans. Circuits Syst., vol.37, no.1, pp.1–9, Jan. 1990.

[6] F. Dartu and L.T. Pileggi, “Calculating worst-case gate delays due to dominant capacitance coupling,” Proc. ACM Design Automation Conference, pp.46–51, June 1997.

[7] J.A. Davis and J.D. Meindl, “Compact distributed RLC interconnect models,” IEEE Trans. Electron Devices, vol.47, no.11, pp.2068–2087, Nov. 2000.

[8] D.D. Antono, K. Inagaki, H. Kawaguchi, and T. Sakurai, “Trends of on-chip interconnects in deep sub-micron VLSI,” IEICE Trans. Electron., vol.E89-C, no.3, pp.392–394, March 2006.

[9] D.D. Antono, K. Inagaki, H. Kawaguchi, and T. Sakurai, “Simple waveform model of inductive interconnects by delayed quadratic transfer function with application to scaling trend of inductive effects in VLSI’s,” IEICE Trans. Fundamentals, vol.E89-A, no.12, pp.3569–3578, Dec. 2006.

[10] T. Sakurai, “Closed-form expressions for interconnection delay, coupling and crosstalk in VLSIs,” IEEE Trans. Electron Devices, vol.40, no.1, pp.118–124, Jan. 1993.

[11] W.C. Elmore, “The transient response of damped linear networks with particular regard to wideband amplifiers,” J. Appl. Phys., vol.19, pp.55–63, Jan. 1948.

[12] MATLAB home page, http://www.mathworks.com/

[13] L.T. Pillage and R.A. Rohrer, “Asymptotic waveform evaluation for timing analysis,” IEEE Trans. Comput.-Aided Des. Integr. Circuits Syst., vol.9, no.4, pp.352–366, Sept. 1990.

Appendix

A.1 Fitting Equation (16)

To modify (15) and obtain (16), we chose aC_J^b as a fitting term and added the fitting terms to (15), so that (16) becomes (15) when C_J=0. Note that a and b are the fitting parameters. We tried the following equations and several other combinations as fitting equations, among which (16) has the least relative error in terms of line delay;

$$v_1(l,t) = E_1 - \frac{1}{n+1}\left\{(E_1 + nE_2)\exp\left[-\frac{t/(RC) - 0.1 - a_1\sqrt{R_T C_J}}{R_T(C_T + a_2 C_J) + R_T + C_T + 0.4}\right] + n(E_1 - E_2)\exp\left[-\frac{t/(RC) - 0.1p - a_1 p\sqrt{R_T C_J}}{R_T(C_T + a_2 C_J) + pR_T + C_T + 0.4p}\right]\right\}, \tag{A·1}$$

where the relative error is 9.6% when n=1, a_1=0.05, and a_2=1.1. The relative error becomes 9.7% when n=2, a_1=0.05, and a_2=1.09.

$$v_1(l,t) = E_1 - \frac{1}{n+1}\left\{(E_1 + nE_2)\exp\left[-\frac{t/(RC) - 0.1 - a_1 R_T C_J}{R_T(C_T + a_2 C_J) + R_T + C_T + 0.4}\right] + n(E_1 - E_2)\exp\left[-\frac{t/(RC) - 0.1p - a_1 R_T C_J}{R_T(C_T + a_2 C_J) + pR_T + C_T + 0.4p}\right]\right\}, \tag{A·2}$$

whose relative error reaches 10.7% when a_1=0.2 and a_2=0.83 in both the two-line and three-line systems.

A.2 Fitting Equation (43)

To obtain (43), we added aR_T^b, aC_T^b, and/or aC_J^b to (42) as fitting terms so that (43) becomes (42) when $R_T = C_T = C_J = 0$. Although we assayed the following equations and more than twenty combinations, (43) exhibits the least absolute error among them in terms of crosstalk noise amplitude;

$$\frac{v_{p,oppo}}{E} = \frac{n\sqrt{p} - n}{n\sqrt{p} + 1 + d_1 C_T + d_2 R_T C_J} \cdot \frac{R_T + R_T C_T + 1}{d_3 R_T + d_4 R_T C_T + 1}, \tag{A·3}$$

where the absolute error is 0.121E (12.1%) when n=1, d_1=1.38, d_2=0.12, d_3=2.29, and d_4=0.59. The absolute error becomes 0.152E (15.2%) when n=2, d_1=1.29, d_2=0.19, d_3=1.78, and d_4=1.18.

$$\frac{v_{p,oppo}}{E} = \frac{n\sqrt{p} - n}{n\sqrt{p} + 1 + d_1\sqrt{C_T} + d_2\sqrt{C_J}} \cdot \frac{\sqrt{R_T} + 1}{d_3\sqrt{R_T} + 1} \cdot \frac{\sqrt{R_T C_T} + 1}{d_4\sqrt{R_T C_T} + 1} \cdot \frac{\sqrt{R_T C_J} + 1}{d_5\sqrt{R_T C_J} + 1}, \tag{A·4}$$

where the absolute error is 0.099E (9.9%) when n=1, d_1=1.7, d_2=0.25, d_3=1.85, d_4=0.91, and d_5=1.31. The absolute error becomes 0.126E (12.6%) when n=2, d_1=3.23, d_2=0.5, d_3=1.54, d_4=0.76, and d_5=1.3.

A.3 Best-Case Delay in Same-Direction Drive

Figure 8 shows that the best-case delay happens in the in-phase drive case. The best-case delay might be considered for a setup time at a flip-flop or something, but it can be theoretically obtained by setting η to zero as mentioned at the beginning of Sect. 3.2. In other words, the worst-case expression in the same-direction drive case includes the best-case one in nature, and it can be easily obtained by substituting $\eta \to 0$.

A.4 Best-Case Delay in Opposite-Direction Drive

In the estimation of the best-case delay, we set $E_1 \to E$ and $E_2 \to E$ in (49), which is as follows;

$$\begin{cases} M_0/(RC) = E\{2R_T C_T + 2R_T C_J + 2R_T + 2C_T + 1\}/2 \\ M_1/(RC)^2 = E\{2n\eta(2C_T + 1) \\ +24R_T^2 C_T^2 + 48R_T^2 C_T + 48R_T C_T^2 + 24R_T^2 + 60R_T C_T \\ +24C_T^2 + 20R_T + 20C_T + 5\}/24 \end{cases}. \tag{A·5}$$

From (48), the best-case delay is obtained as follows;

$$\begin{aligned} t_{pd,oppo}/(RC) &= \{2R_T C_T + 2R_T C_J + 2R_T + 2C_T + 1\}/2 \\ &\quad - \ln[e/2]\sqrt{}\left[n\eta(2C_T + 1) + 6R_T^2 C_T^2 - 12R_T^2 C_T C_J\right. \\ &\quad -6R_T^2 C_J^2 + 12R_T^2 C_T - 12R_T^2 C_J + 12R_T C_T^2 - 12R_T C_T C_J \\ &\quad \left.+ 6R_T^2 + 12R_T C_T - 6R_T C_J + 6C_T^2 + 4R_T + 4C_T + 1\right]/\sqrt{6} \\ &\approx \frac{\ln[e/2]}{2\sqrt{6}} n\eta(6R_T C_T C_J - 2R_T C_T - 3R_T C_J + 2R_T - 1) \\ &\quad + \left(1 - \frac{2\ln[e/2]}{\sqrt{6}}\right)(R_T C_T + R_T + C_T) \\ &\quad + \left(1 + \frac{3\ln[e/2]}{\sqrt{6}}\right)R_T C_J + \frac{1}{2} - \frac{\ln[e/2]}{\sqrt{6}} \\ &= 0.06n\eta(6R_T C_T - 2R_T C_T - 3R_T C_J + 2R_T - 1) \\ &\quad +0.75(R_T C_T + R_T + C_T) + 1.38R_T C_J + 0.37 \\ &= b_1 n\eta(6R_T C_T - 2R_T C_T - 3R_T C_J + 2R_T - 1) \\ &\quad +b_2(R_T C_T + R_T + C_T) + b_3 R_T C_J + b_4. \end{aligned} \tag{A·6}$$

where b_1, b_2, b_3, and b_4 are fitting parameters. Unfortunately, no matter what values are chosen as the fitting parameters, the relative error of (A·6) always becomes 100% unless $b_1 = b_4 = 0$. This is because the best-case delay becomes zero if $R_T = C_T = C_J = 0$ and η is two or more. In this case, the waveform goes beyond $E/2$ at the moment of t=0 (suppose η is two or more, and apply it to the best-case delay in Fig. 15). However, the parameter setting that $b_1 = b_4 = 0$ is not appropriate, which implies that (A·6) based on the first-order moment matching is not suitable for the best-case delay derivation.

Hiroshi Kawaguchi received the B.E. and M.E. degrees in electronic engineering from Chiba University, Chiba, Japan, in 1991 and 1993, respectively, and the Ph.D. degree in engineering from the University of Tokyo, Tokyo, Japan, in 2006. He joined Konami Corporation, Kobe, Japan, in 1993, where he developed arcade entertainment systems. He moved to the Institute of Industrial Science, the University of Tokyo, as a Technical Associate in 1996, and was appointed a Research Associate in 2003. In 2005, he move to the Department of Computer and Systems Engineering, Kobe University, Kobe, Japan, as a Research Associate. Since 2007, he has been an Associate Professor with the Department of Computer Science and Systems Engineering, Kobe University. He is also a Collaborative Researcher with the Institute of Industrial Science, the University of Tokyo. His current research interests include low-power VLSI design, hardware design for wireless sensor network, and recognition processor. Dr. Kawaguchi was a recipient of the IEEE ISSCC 2004 Takuo Sugano Outstanding Paper Award and the IEEE Kansai Section 2006 Gold Award. He has served as a Program Committee Member for IEEE Symposium on Low-Power and High-Speed Chips (COOL Chips), and as a Guest Associate Editor of IEICE Transactions on Fundamentals of Electronics, Communications and Computer Sciences. He is a member of the IEEE and ACM.

Danardono Dwi Antono was born in Jakarta, Indonesia in 1977. He received the degrees of B.Eng., M.Eng., and Ph.D. in electronic engineering from the University of Tokyo in 2001, 2003, and 2006, respectively. His research interest covered interconnects modeling and signal integrity on VLSIs. Since April 2006, he has been with Sony Corporation, and has engaged on the field of System LSI. He is a member of IEEE.

Takayasu Sakurai received the Ph.D. degree in EE from the University of Tokyo, Tokyo, Japan, in 1981. In 1981, he joined Toshiba Corporation, where he designed CMOS DRAM, SRAM, RISC processors, DSPs, and SoC Solutions. He has worked extensively on interconnect delay and capacitance modeling known as Sakurai model and alpha power-law MOS model. From 1988 through 1990, he was a visiting researcher at the University of California Berkeley, where he conducted research in the field of VLSI CAD. From 1996, he has been a Professor at the University of Tokyo, working on low-power high-speed VLSI, memory design, interconnects, ubiquitous electronics, organic IC's and large-area electronics. He has published more than 350 technical publications including 70 invited publications and several books and filed more than 100 patents. He served as a conference chair for the Symposium on VLSI Circuits, and ICICDT, a vice chair for ASPDAC, a TPC chair for the first A-SSCC, and VLSI Symposium and a program committee member for ISSCC, CICC, DAC, ESSCIRC, ICCAD, FPGA workshop, ISLPED, TAU, and other international conferences. He is a plenary speaker for the 2003 ISSCC. He is a recipient of 2005 IEEE ICICDT award, 2005 IEEE ISSCC Takuo Sugano award and 2005 P&I patent of the year award. He is an IEEE Fellow, a STARC Fellow, an elected AdCom member for the IEEE Solid-State Circuits Society and an IEEE CAS distinguished lecturer.